Journal of Non-Crystalline Solids 355 (2009) 991–1000

Contents lists available at ScienceDirect

Journal of Non-Crystalline Solids

journal homepage: www.elsevier.com/locate/jnoncrysol

Doping of a high calcium oxide metaphosphate glass with titanium dioxide

Ensanya A. Abou Neel [a], Wojciech Chrzanowski [a,1], Sabeel P. Valappil [a,2], Luke A. O'Dell [b], David M. Pickup [c], Mark E. Smith [b], Robert J. Newport [c], Jonathan C. Knowles [a,*]

[a] Division of Biomaterials and Tissue Engineering, UCL Eastman Dental Institute, 256 Gray's Inn Road, London WC1X 8LD, UK
[b] Physics Department, University of Warwick, Coventry CV4 7AL, UK
[c] School of Physical Sciences, University of Kent, Canterbury CT2 7NH, UK

ARTICLE INFO

Article history:
Received 26 September 2008
Received in revised form 5 March 2009
Available online 4 May 2009

PACS:
82.80.Bg
61.43.Fs
82.80.Pv
76.60.-k

Keywords:
Bioglass
Biomaterials
Chemical durability
Glass ceramics
X-ray diffraction
Glass transition
FTIR measurements
NMR, MAS-NMR and NQR

ABSTRACT

This study investigates the effect of doping a high calcium oxide containing metaphosphate glass series $(CaO)_{40}(Na_2O)_{10}(P_2O_5)_{50}$ with TiO_2 (1, 3, and 5 mol%). TiO_2 incorporation increased the density and glass transition temperature while reduced the degradation rate (5 mol% in particular) by twofold compared with $(CaO)_{30}$ system reported previously. This has been confirmed by ion release and the minimal pH changes. TiP_2O_7, $NaCa(PO_3)_3$ and CaP_2O_6 phases were detected for all TiO_2-containing ceramics. XPS showed that the surface is composed of Ca, P, and Ti. Ti was recognized mainly as TiO_2, but its total amount was lower than theoretical values. ^{31}P magic angle spinning (MAS) NMR showed a downfield shift of the ^{31}P lineshape with increasing TiO_2, interpreted as an effect of the titanium cation rather than an increase in the phosphate network connectivity. FTIR showed that incorporation of TiO_2 increased the strength of the phosphate chains, and the O/P ratio while introducing more Q^1 units into the structure at the expense of the Q^2 units. There were no differences, however, in surface topography roughness and free energies between these glasses. These results suggested that TiO_2 and CaO were acting synergistically in producing glasses with controllable bulk and structural properties.

1. Introduction

Bioactive and bioresorbable biomaterials that can stimulate specific and controlled cell responses at the molecular level are now of major interest as scaffolds for tissue engineering [1]. Phosphate glasses based on the ternary P_2O_5–CaO–Na_2O system have the potential to be used as scaffold materials. They are degradable and the degradation rate is strongly dependant on composition, and accordingly a wide range of materials with different degradation rates can be obtained by tailoring the glass chemistry [2–4]. Furthermore, their degradation products can be eliminated by the normal physiological mechanisms of the body [5].

Several attempts have been made in order to harmonize the degradation behavior with the end application. For example, substituting Na_2O with CaO yielded glass systems that were less degradable, since Ca^{2+} ions have much stronger field strengths than Na^+ and a chelating structure could be formed with ionic bonding between two adjacent phosphate tetrahedra [6,7]. The degradation can also be reduced by an increase of the cross-linkage or the introduction of highly insoluble ions, which makes the glass structure less susceptible to solution attack [8]. Reducing the degradation in turn has led to better biocompatibility [9], for instance, an enhanced bone cell growth together with an up regulation of antigen expression has been observed [10]; in addition, a minimal inflammatory response was also induced by the extracts of low soluble glasses [11,12].

Titanium dioxide (TiO_2) has been used previously for the production of bioactive and biocompatible phosphate-based glasses. TiO_2 acts as a nucleating agent, and although it is miscible in the molten glass, it induces phase separation during cooling of the melt. It was observed that the addition of 0.5 mol% TiO_2 enhanced the bioactivity which started to decrease upon further increase of the TiO_2 content [13].

In our previous study, it has been shown that the addition of TiO_2 into $(CaO)_{30}(Na_2O)_{20}(P_2O_5)_{50}$ phosphate glasses improved the cellular

* Corresponding author. Tel.: +44 (0) 207 915 1189; fax +44 (0) 207 915 1227.
E-mail address: j.knowles@eastman.ucl.ac.uk (J.C. Knowles).
[1] Present address: University of Glasgow, Mechanical Engineering Department, James Watt South Building, G12 8QQ Glasgow, UK.
[2] Present address: School of Dental Sciences, University of Liverpool, Liverpool L69 3GN, UK.

0022-3093/$ - see front matter © 2009 Elsevier B.V. All rights reserved.
doi:10.1016/j.jnoncrysol.2009.04.016

response by adjusting the glass degradation [14]. Therefore, it was assumed that TiO_2-containing glasses that maintain the TiO_2 at 1, 3, and 5 mol% and increasing the CaO content (to 40 mol%) could further improve the cellular response by introducing further control of their degradation. Metaphosphate glasses with high calcium content have already been shown to be better for cellular proliferation than those with low calcium content [9]. Hence, the aims of this study were; (a) to prepare glasses of the general formula $(CaO)_{40}(Na_2O)_{10-x}(P_2O_5)_{50}(TiO_2)_x$, where $x = 0$, 1, 3 and 5, (b) analyze the thermal and structural properties of these glasses using differential scanning calorimetry (DSC), differential thermal analysis (DTA), X-ray powder diffraction (XRD), X-ray photoelectron spectroscopy (XPS), nuclear magnetic resonance, and FTIR spectroscopy (c) conduct *in vitro* studies on glass degradation, ion release, and pH changes of the degrading medium and (d) to correlate these results to surface properties; roughness, wettability and surface free energy of the glasses.

2. Experimental

2.1. Manufacture of the glasses

Glass rods of 15 mm diameter were prepared using NaH_2PO_4, $CaCO_3$, P_2O_5 and TiO_2 (all chemicals were >98% purity,) as precursors by the conventional melt quenching process at the corresponding temperatures and time given in Table 1. Each rod was then sectioned into approximately 1 mm thick discs using a diamond saw with methanol as a coolant/lubricant. These discs were then subjected to a series of grinding and polishing steps using waterproof silicon carbide papers; P# 120 for 30 s at 300 RPM to flatten the surface, then P# 500, 1000, 2400, respectively, for 1 min at 500 RPM to smooth the surfaces, and finally P# 4000 for 2 min to get a smooth mirror-finish surface on a Struers Rotopol-11. These discs were used for density, degradation and surface free energy measurements. However, powdered samples, prepared by grinding pieces of glasses in an agate mill, were used thermal, NMR, and FTIR studies. Crystalline powdered samples were used for XRD.

2.2. Bulk glass characterization

2.2.1. Density measurements

Density measurements were conducted on triplicate samples using Archimedes' Principle, on an analytical balance with an attached density kit with ethanol as the immersion liquid for these measurements.

2.2.2. Thermal characterization

Thermal characterization was carried out using both Pyris Diamond DSC and Setaram Differential Thermal Analyzer as previously described (18) to determine glass transition (T_g) crystallization (T_c), and melting temperatures (T_m) at a heating rate of 20 °C min^{-1}.

2.2.3. Degradation studies

The surface area of the glass discs were calculated from the dimensions obtained with Mitutoyo Digimatic Vernier Callipers. Three glass discs from each composition were used for this experiment. They were placed in glass bottles containing 25 ml of high purity water (18.2 MΩ cm resistivity) obtained from PURELAB UHQ-PS with the pH adjusted to 7 ± 0.2 using few drops of NH_4OH. At various time points (0.25, 1, 5, 12, 19, and 26 days), the solutions were removed for ion release analysis. Simultaneously, the discs were taken out of their respective containers, blot dried with tissue and weighed to assess the weight loss. The discs were then placed in a fresh solution of high purity water and placed back into the incubator at 37 °C. Applying a weight loss method [3,4] to these data, a plot of cumulative degradation (% weight loss per unit area) as a function of time was produced.

2.2.4. pH measurements

At every time point pH measurements were taken after transferring the glass discs to a fresh solution (high purity water, pH 7 ± 0.2). The measurements were collected using a Hanna Instruments pH 211 Microprocessor pH meter with attached glass combination pH electrode. This electrode was calibrated using pH colorkey buffer solutions.

2.2.5. Ion release measurements

Ion release studies were simultaneously conducted, and the medium was analyzed for cation (Ca^{2+} and Na^+) and anion (PO_4^{3-}, $P_2O_7^{4-}$, $P_3O_9^{3-}$, and $P_3O_{10}^{5-}$) release by ion chromatography. Inductively coupled plasma mass spectrometry (ICP-MS) was used to determine the amount of Ti^{4+} ions released from all glass compositions at the previously mentioned time points. The instrument was calibrated using the ICP multi-element standard V diluted in ultrapure water to a range of 1–800 ppb, and the Ti^{4+} concentration in the ultrapure water was set as 0 ppb.

2.3. Structural characterization

2.3.1. X-ray powder diffraction

For X-ray powder diffraction (XRD) analysis, the powdered samples were annealed in a ceramic pot from room temperature to the corresponding crystallization temperature, obtained from the differential thermal analyzer, at a heating rate of 20 °C min^{-1} using Lenton Furnace. The temperature was maintained at this temperature for three hours to ensure proper crystallization, and finally it was reduced to room temperature at the same rate used for heating. The data was collected on Brüker D8 Advance Diffractometer in flat plate geometry, using Ni filtered Cu Kα radiation and a Brüker Lynx Eye detector. Data was collected from 10° to 100° 2θ with a step size of 0.02° and a count time of 0.1 s. The phases were identified using the Crystallographica Search-Match (CSM) software and the International Center for Diffraction Data (ICDD) database (vols. 1–42).

2.3.2. X-ray photoelectron spectroscopy

The surface chemical composition of the glass samples with increasing titanium content was measured using X-ray photoelectron spectroscopy (XPS) (Thermo Escalab 220iXL). Measurements

Table 1
Glass codes, melting regime used, the calculated density (ρ) in g cm^{-3}, and glass transition temperature (T_g) in °C.

Glass code	Glass composition (mol%)					Processing temperature		Properties	
	Notation	Calcium oxide	Sodium oxide	Phosphorus pentoxide	Titanium dioxide	Melting temperature (°C)/time (h)	Annealing temperature (°C)/time (h)	ρ (g cm^{-3})	T_g (°C)
$(CaO)_{40}(Na_2O)_{10}(P_2O_5)_{50}$	CNP	40	10	50	0	1100/1	350/1	2.62 ± 0.00	459 ± 2
$(CaO)_{40}(Na_2O)_9(P_2O_5)_{50}(TiO_2)_1$	CNPT1	40	9	50	1	1300/1	420/1	2.64 ± 0.01	479 ± 2
$(CaO)_{40}(Na_2O)_7(P_2O_5)_{50}(TiO_2)_3$	CNPT3	40	7	50	3	1300/3	420/1	2.65 ± 0.00	506 ± 1
$(CaO)_{40}(Na_2O)_5(P_2O_5)_{50}(TiO_2)_5$	CNPT5	40	5	50	5	1300/3	420/1	2.67 ± 0.00	518 ± 0.4

were performed using an Al Kα monochromated X-ray source and quantified with CasaXPS. Before the measurement, the surface was polished with SiC paper (grid 500–4000), ultrasonicated in methanol for 10 min and dried with compressed air. For all the samples, both survey and high resolution spectra were recorded to enable precise evaluation of the chemical composition. Due to the non-conductive properties of the glasses, to allow accurate analysis of the chemical composition for all samples a silver mask and flood gun were used to compensate charge.

2.3.3. FTIR spectroscopy

FTIR spectra were recorded in transmission mode on a Biorad FTS175C spectrometer controlled by Win-IR software. Samples were diluted in dry KBr, pressed into 13 mm diameter disks and scanned in the range 4000–450 cm^{-1} with a resolution of 4 cm^{-1}. Each spectrum was the result of summing 64 scans.

2.3.4. Nuclear magnetic resonance

^{23}Na magic angle spinning (MAS) NMR experiments were conducted using a 4 mm diameter rotor spinning at 12.5 kHz. Aqueous NaCl was used as a reference, with the sharp resonance from this set to 0 ppm. The liquid 90° pulse length was determined to be 2.5 μs, although a much shorter pulse length (0.5 μs) was used on the solid samples. A one-pulse sequence was used, with a pre-acquisition delay of 5.0 μs, a recycle delay of 5 s which was sufficient to produce a fully relaxed spectrum.

^{31}P MAS NMR experiments were also conducted using a 4 mm diameter rotor spinning at 12.5 kHz. Solid $NH_4H_2PO_4$ was used as a secondary reference compound, the signal from this set to 0.9 ppm. A pulse length of 1.5 μs was used (corresponding to a ~30° tip angle), with a recycle delay of 5 s, sufficient to produce relaxed spectra.

NMR spectra were acquired using a Chemagnetics Infinity Plus spectrometer attached to a 7.05 T magnet (^{23}Na Larmor frequency 79.36 MHz and ^{31}P Larmor frequency 121.5 MHz). One ^{23}Na spectrum was acquired at 18.8 T (^{23}Na Larmor frequency 211.4 MHz) using a 4 mm probe and similar experimental conditions as above. Spectra were subsequently processed using Spinsight and simulated using Dmfit [15] or QuadFit [16].

2.4. Substrate surface characterization

2.4.1. Surface roughness

Topography of the surface was examined using atomic force microscope (AFM) (PSIA, XE-100). Images of the surface were recorded using non-contact mode with a silicon tip and the scan rate was 1 Hz. For all samples, three sizes of images were recorded: 10 × 10 μm, 25 × 25 μm and 45 × 45 μm. The roughness parameter R_a was assessed on the line profiles obtained from the 45 × 45 μm images. However, it must be highlighted that the cut-off length for AFM measurements is significantly shorter than the length given by the standard (DIN 4768, ISO 4288). These measurements represent 'nanoscale roughness'. For this reason, laser profilometry measurements (Proscan 1000, Scantron) were also conducted to provide information on the 'macroscale' R_a values. The cut-off length was $\lambda_c = 0.8$ mm and evaluation length was 4 mm. Due to the transparent nature of the samples, replicas were prepared using MicroSET (Microset Products Limited, UK), and the measurements were carried out on the replicas. To obtain replica, two microset components were applied onto the samples surface using dispensing gun. Some pressure was applied on the material with cover slip, and left until the components were set. The replicas were separated from the samples and examined using laser profilometer. Nevertheless, the replicas technique enables the reproduction of features on the surface greater then 0.1 μm, which in turn can affect the roughness results.

2.4.2. Wettability and surface free energy

Surface free energy (SFE) was evaluated on the basis of contact angle measurements using polar and non-polar liquids (ultrapure water and diiodomethane) using a KSV200 (KSV) instrument. Droplets of approximately 2.5 μl of ultra-pure water and diiodomethane were placed on the glass surface using a motorized syringe. The drop profile was recorded at 1 s intervals for 1 min, and the measurements were carried out in triplicate.

2.5. Statistical analysis

The *t*-test was used to study the effect of TiO_2 content on density, glass transition temperature, contact angle and surface free energy. Significance was detected at a 0.05 level, and all statistical analysis was carried out using the SPSS system for Windows (SPSS 12.0.1).

3. Results

3.1. Bulk glass characterization

3.1.1. Density

Replacement of Na_2O with TiO_2 produced glasses with significantly higher density which increased from 2.62 g cm^{-3} for TiO_2-free glass (CNP) to 2.67 g cm^{-3} for 5 mol% TiO_2-containing glasses (CNPT5) as given in Table 1.

3.1.2. Thermal characterization

The increase in density was also associated with an increase in T_g that increased from 459 ± 2 for CNP to 518 ± 2 °C for CNPT5 glasses as in Table 1.

The DTA trace of the CNP was characterized by the presence of a single sharp crystalline peak at 600 °C and two melting peaks at 757 and 864 °C. The crystalline phase obtained for 1 mol% TiO_2-containing glass (CNPT1) was observed at 650 °C, and the two melting peaks were identified at 756 and 866 °C. Incorporation of 3 mol% TiO_2 produced a shift in the crystallization to higher temperature 683 °C, and the melting peaks were identified at 750 and 894 °C. A second crystalline peak was only observed by addition of 5 mol% TiO_2 into the ternary CNP glasses. A shift in the crystallization peaks to higher temperatures was also observed for the 5 mol% TiO_2-containing glass, CNPT5 (720 and 750 °C), with the melting peak was identified at 910 °C as in Fig. 1.

3.1.3. Degradation studies

Fig. 2 shows the cumulative degradation (weight loss per unit area) as a function of time for all tested glass samples. The weight loss per unit area increased with time in all cases and decreased with increasing TiO_2 content in the glass structure. For comparison purposes, the degradation rate was calculated by applying a line of

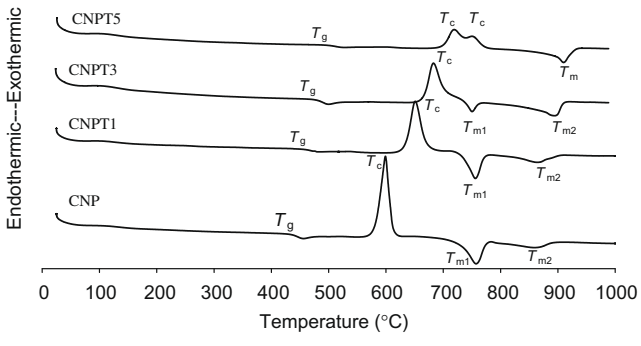

Fig. 1. DTA trace for glasses with different TiO_2 contents.

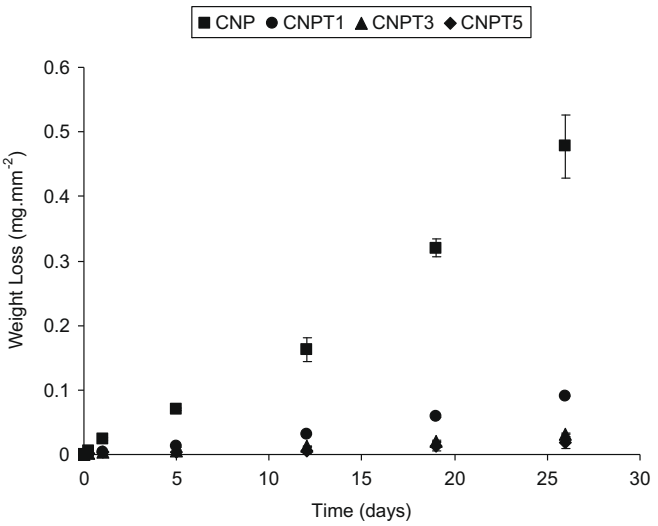

Fig. 2. Degradation profiles, presented as cumulative weight loss/surface area, for CNPT1, CNPT3, and CNPT5 compared to CNP glass as a control as a function of time.

best fit through the weight loss per unit area of each glass against time, and it was 17.42, 3.33, 0.98 and 0.81 μg mm^{-2} h^{-1} for CNP, CNPT1, CNPT3, and CNPT5, respectively. As can be seen, all the TiO_2-containing glasses (CNPT1, CNPT3, and CNPT5) showed perceptible differences in their degradation rate profiles compared to TiO_2-free glasses (CNP). Moreover, the degradation rates were found to decrease with an increasing TiO_2 content; it was reduced by one order of magnitude with incorporation of 1 mol% TiO_2 while the incorporation of 3 and 5 mol% TiO_2 reduced it by two orders of magnitude.

3.1.4. pH changes

Fig. 3 shows the pH changes of deionized water used for the degradation studies as a function of time for all glass compositions tested. As can be seen, the CNP glasses displayed the greatest decrease (4.92) in pH of the surrounding medium from the initial value of 7. The pH for the medium surrounding CNPT1, CNPT3, and CNPT5 remained closer to the starting pH throughout the duration of the study.

3.1.5. Cumulative ion release measurements

The cumulative release pattern for both Na^+ and Ca^{2+} follow the same trend as the degradation with CNP releasing the highest level

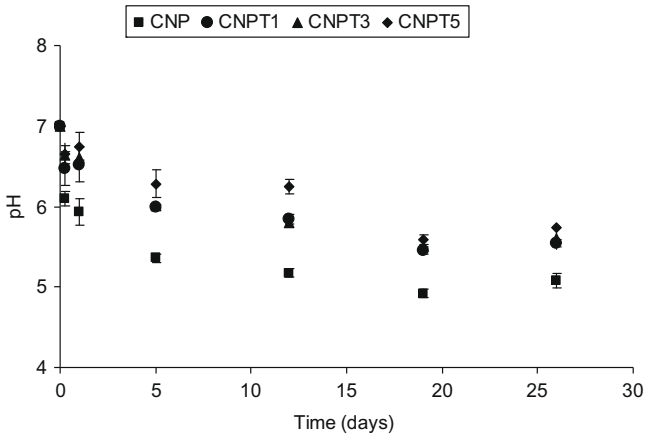

Fig. 3. pH change in deionized water as a function of time for CNPT1, CNPT3, and CNPT5 compared to CNP glass as a control.

of both cations, and the level of such release decreased with increasing TiO_2 content in the glass structure. The level of both Na^+ and Ca^{2+} release was of the same order of magnitude. The rate of release of these cations was also calculated in the same way as presented previously for the degradation as shown in Fig. 4(a). Both the Na^+ and Ca^{2+} release rates displayed statistically significant ($P \leqslant 0.0001$) differences between CNPT1 compared to CNPT3 and CNPT5 and also between CNPT3 and CNPT5 glasses. It can be seen that compositions with higher mol% sodium released more Na^+ ions into solution, and this release was directly proportional to the degradation rate values. The greatest Na^+ release was seen for the CNP composition, with a statistically significant ($P \leqslant 0.0001$) difference seen between this composition and CNPT1, CNPT3, and CNPT5 compositions.

The cumulative release pattern for all anion species appears to be linear in nature, as was the case with both cations. Among the anions (PO_4^{3-}, $P_2O_7^{4-}$, $P_3O_9^{3-}$ and $P_3O_{10}^{5-}$), $P_3O_9^{3-}$ was the anion released to the greatest extent followed by $PO_4^{3-} > P_3O_{10}^{5-} > P_2O_7^{4-}$. The rate of anion release showed a statistically significant ($P \leqslant 0.0001$) difference between CNPT1 compared to CNPT3 and CNPT5 compositions and also between CNPT3 and CNPT5 glasses ($P \leqslant 0.0417$) as shown in Fig. 4(b). The profiles of both cation and anion release rates were found to correlate strongly with the rate of glass degradation.

The cumulative release of Ti^{4+} found to be inversely proportional to the TiO_2 content in the glasses with CNPT1 releasing the maximum followed by CNPT3 and CNPT5 glasses, and correlated well with the degradation. As expected, there was no Ti^{4+} release from CNP (Fig. 4).

3.2. Structural characterization

3.2.1. X-ray powder diffraction

The main phase identified for CNP was found to be sodium calcium phosphate [$NaCa(PO_3)_3$-23-669], with a secondary phase of β-calcium phosphate [β-$Ca(PO_3)_2$-17-500] was also observed. For CNPT1, CNPT3, and CNPT5, calcium phosphate [CaP_2O_6-11-39] was the main phase, while [$NaCa(PO_3)_3$-23-669], and titanium phosphate [TiP_2O_7-38-1468] were detected as secondary phases.

3.2.2. X-ray photoelectron spectroscopy

Results of surface chemical composition analysis of the glass samples are complied in Table 2. In addition to the expected oxides, the glass surfaces were found to be contaminated with 15–30 wt% carbon and 1.5–3.0 wt% nitrogen. Analysis of the binding energies showed the elements (C, Ca, N, Na, O, P and Ti) which were found in the samples, and enabled assessment of the content and forms of these elements.

For the CNP, the carbon line (C1s) has three main peaks (Fig. 5(a)). The dominant peak at the energy Eb = 284.4 eV corresponds to graphite. The second peak was observed at Eb = 286.0 eV, which was recognized as single bonded carbon C–C, and it is usually related to contaminants. A third peak was observed at higher energy (Eb = 288.9 eV), and this corresponds to carbon double-bonded to oxygen C=O. Calcium with a total content about 6% was observed as an oxide CaO – Eb = 347.4 eV (Fig. 5(b)). Also some nitrogen approximately 2%, some bonded to oxygen (i.e. N–O Eb = 399.7 eV) and other bonded to carbon C–N (Eb = 401.6 eV) was found (Fig. 5(c)). Sodium was observed as a metal Na (Eb = 1071.5 eV) (Fig. 5(d)), with the width of the sodium peak suggesting that some of the sodium was also associated with $NaPO_4$ (1071.6 eV). The region associated with oxygen line has two dominant peaks at energies 531.3 and 532.6 eV (Fig. 5(e)), which suggest the presence of –OH groups, and oxygen–carbon bonds, e.g., O–C, C=O. Phosphorus was recognized as P_2O_5 (Eb = 133.9 eV), but it was difficult to distinguish between different oxide forms of phosphorus and for this rea-

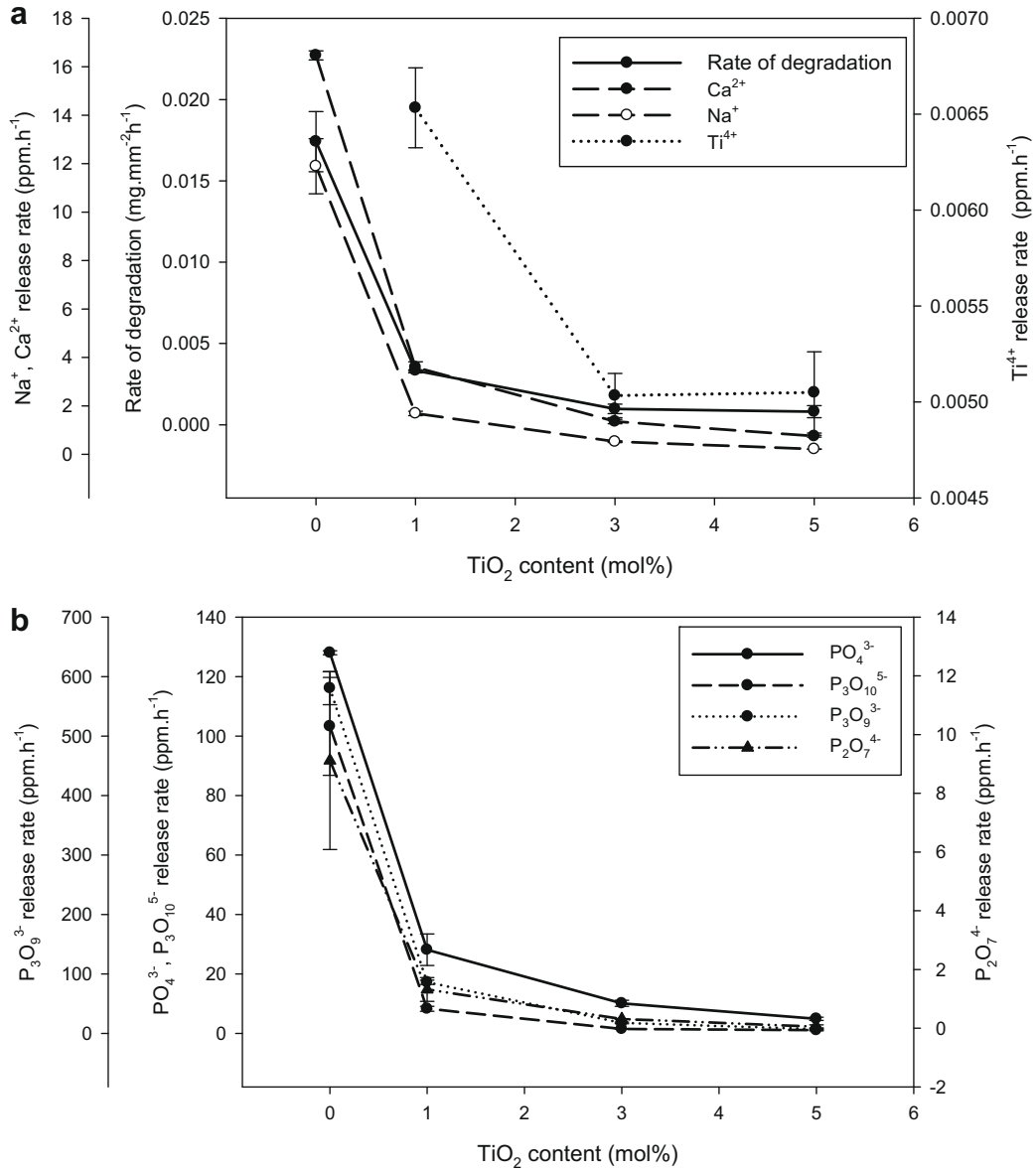

Fig. 4. Rate of degradation, and ion release for different cationic and anionic species as a function of the glass composition: (a) degradation rate, Na^+, Ca^{2+}, and Ti^{4+}, (b) $P_3O_9^3$, PO_4^{3-}, $P_3O_{10}^{5-}$, and $P_2O_7^{4-}$ release rate. The rate was considered by fitting a straight line and forcing it to pass through the origin.

Table 2
Results of chemical composition using XPS (mol%), total surface free energy (SFE^{tot} in mN m^{-1}) with the dispersive (SFE^d) and polar part (SFE^p) according to OWRK method, contact angle measurements (°) for ultra-pure water [CA° (H_2O)] and diiodomethane [CA° (DII)], and roughness obtained from AFM and laser profilometer for studied glasses.

Glass annotation	Chemical composition by XPS (mol%)				Contact angle (°) and surface free energy (mN m^{-1})					Roughness measurements	
	CaO	Na_2O	P_2O_5	TiO_2	CA° (H_2O)	CA° (DII)	SFE^d, mN m^{-1}	SFE^p, mN m^{-1}	SFE^{tot} mN m^{-1}	R_a, nm (AFM)	R_a, μm (profilometer)
CNP	34.1 ± 0.6	20.4 ± 2.4	45.5 ± 0.4	0 ± 0	10.8 ± 2.3	37.3 ± 0.3	40.9 ± 0.16	35.0 ± 0.5	75.9 ± 0.4	5.1 ± 1.0	0.3 ± 0.1
CNPT1	35.7 ± 1.8	16.6 ± 2.7	46.1 ± 2.4	1.5 ± 0.5	09.8 ± 1.1	34.2 ± 1.9	42.4 ± 0.9	34.4 ± 0.3	76.8 ± 0.6	5.8 ± 1.2	0.4 ± 0.1
CNPT3	34.2 ± 0.7	11.8 ± 0.0	49.2 ± 1.4	4.8 ± 0.6	13.5 ± 0.3	33.9 ± 2.6	42.5 ± 1.2	34.0 ± 1.4	76.5 ± 0.5	8.4 ± 1.5	0.4 ± 0.1
CNPT5	35.1 ± 1.3	9.6 ± 4.2	50.5 ± 0.9	4.7 ± 1.2	11.7 ± 3.1	44.3 ± 3.2	39.2 ± 3.4	36.3 ± 1.8	75.5 ± 1.8	4.2 ± 0.1	0.3 ± 0.1

son it should be interpreted as generally referring to phosphorus oxide species and not to any specific form (Fig. 5(f)).

For the CNPT1, CNPT3, and CNPT5 samples, an increase of carbon concentration was observed. There were no changes in shape of main peaks. Calcium, nitrogen and phosphorus content and its form for the titanium-doped samples remained constant. No significant changes in the shape of the oxygen spectra were observed, and the energies of the main oxygen peaks were the same as recorded for CNP. Some differences, however, were observed in titanium and sodium content. The titanium content gradually increased from 0.27% for CNPT1 to 0.83% for CNPT5, and it was mainly recognized as TiO_2 (Eb = 459.3 eV). With increasing titanium content, a decrease of sodium from 4.2% to 1.6% was observed, and the binding energy of the sodium peak remained at Eb = 1071.5 eV, throughout the series.

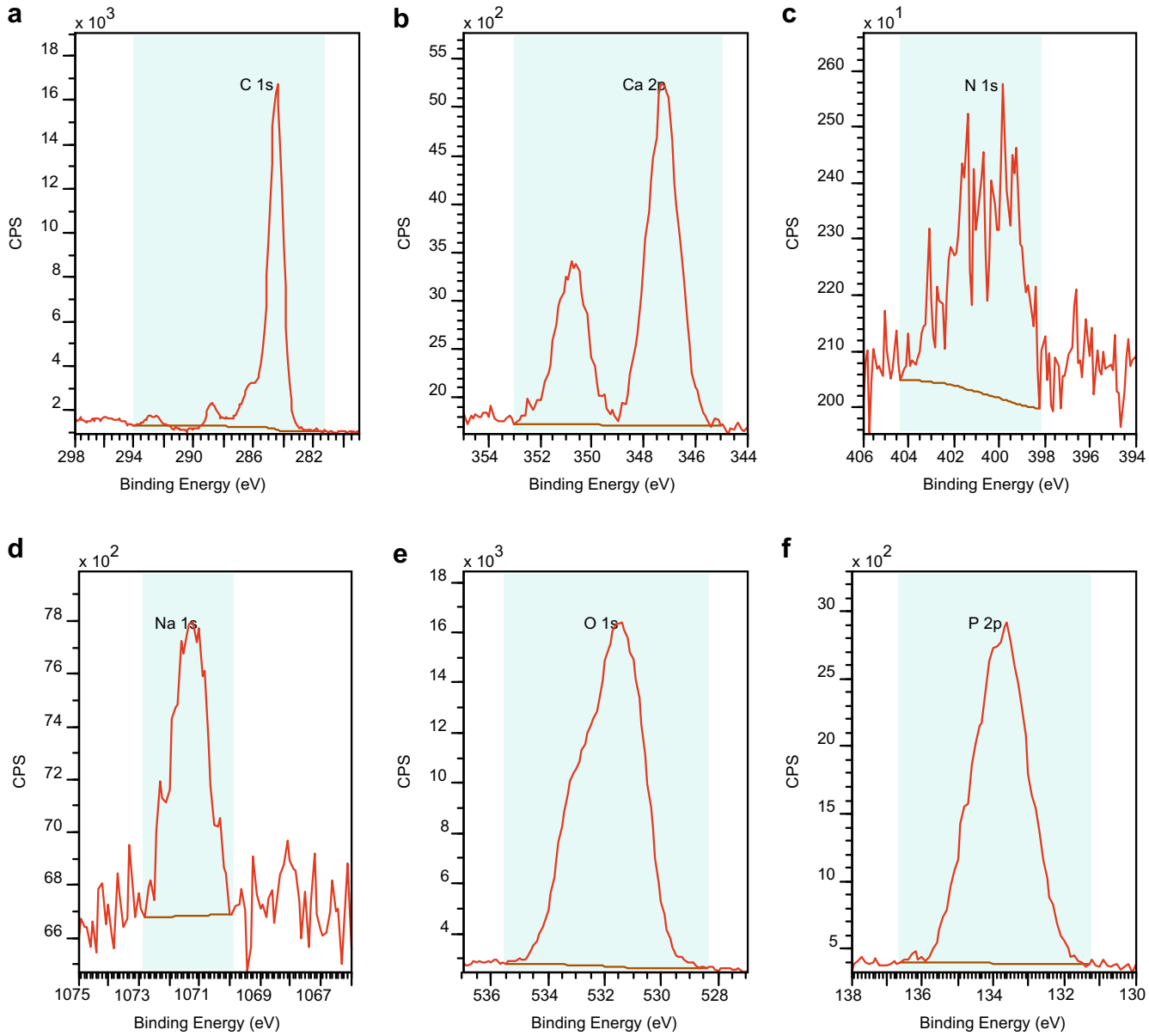

Fig. 5. XPS high resolution spectra of C, Ca, P, Na, N and O CNPT1, CNPT3, and CNPT5 compared to CNP glass as a control.

Table 3
Abbreviations: δ, deformation; ν, stretching; s, symmetric; as, asymmetric.

Wavenumber/cm^{-1}	Assignment[a]	Associated Q^n (where applicable)
540	δ(P–O–P)	
725	ν_s(P–O–P)	
770	ν_s(P–O–P)	
900	ν_{as}(P–O–P)	Q^2
1000	$\nu_s(PO_3)^{2-}$	Q^1
1100	$\nu_{as}(PO_3)^{2-}$	Q^1
1270	$\nu_{as}(PO_2)^-$	Q^2

[a] Refs. [23–26].

3.2.3. FTIR spectroscopy

Great variation is observed between the FTIR spectra from the titanium-doped samples as a function of Ti^{4+} content. It can be seen from the spectra in Fig. 6 that as the Ti^{4+} content increases, the intensity of the bands associated with Q^2 groups at ~1270 and 900 cm^{-1} decrease relative to those associated with Q^1 groups at ~1100 and 1000 cm^{-1}. The absorption bands in the above

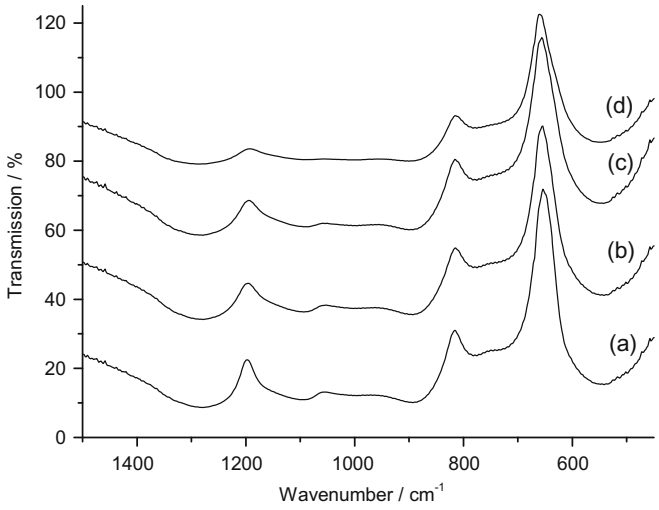

Fig. 6. FTIR spectra from: (a) CNP, (b) CNPT1, (c) CNPT3 and (d) CNPT5.

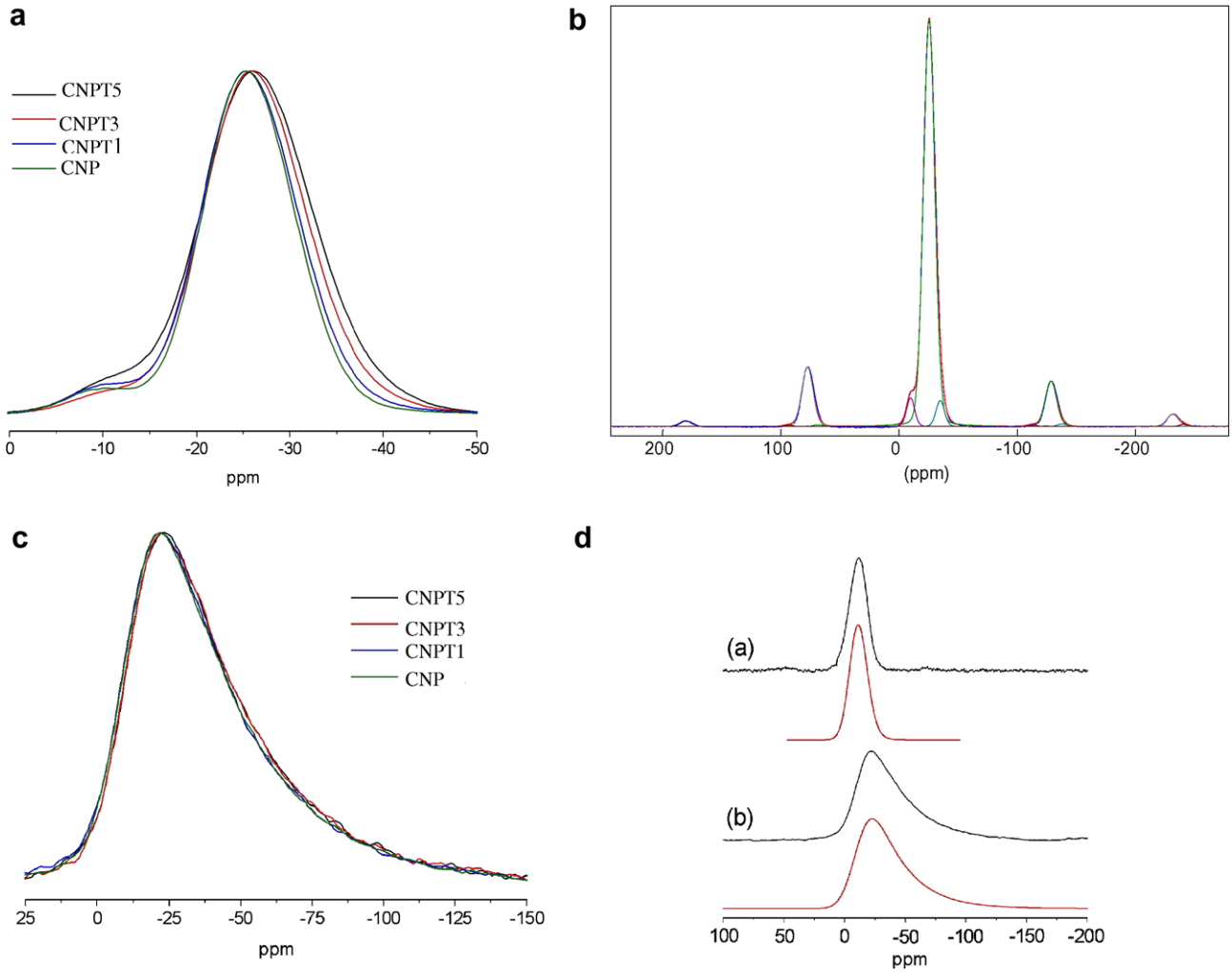

Fig. 7. (a) The overlaid ^{31}P MAS NMR spectra obtained from the samples, with the horizontal frequency scale expanded to show just the isotropic region, (b) fit of the ^{31}P MAS NMR spectrum obtained from the CNPT1 metaphosphate glass, (c) the overlaid ^{23}Na MAS NMR spectra obtained from the samples, with the horizontal frequency scale expanded to show just the isotropic region, (d) the ^{23}Na MAS NMR spectra obtained from the 0 mol% TiO_2 sample at (a) 18.8 T and (b) 7.05 T. Red lines show fits of each spectrum obtained by simulating a distribution in C_Q. (For interpretation of the references to color in this figure legend, the reader is referred to the web version of this article.)

spectra can be assigned according to the data in Table 3 [23–26]. Moreover, a small shift of the ν_{as}(P–O–P) band to higher energy is observed with Ti^{4+} content, as is a general broadening of the spectral features.

3.2.4. Nuclear magnetic resonance

Fig. 7(a) shows the ^{31}P MAS NMR spectra obtained from the glasses, with the horizontal frequency scale expanded about the isotropic region such that the spinning sidebands are not shown. It can be seen that the linewidth increases with increasing TiO_2 content, the centre of gravity of the spectrum shifting downfield. In light of the FTIR results, this lineshape can be interpreted as an increase in Q^1 (using the Q^n notation where n is the number of bridging oxygen atoms of the PO_4 tetrahedron), with the Ti^{4+} cation having the effect of moving the Q^1 phosphorus chemical shift downfield, an effect already observed in the ^{31}P MAS NMR spectrum of TiP_2O_7, which features Q^1 chemical shifts in the range −35 to −50 ppm [17]. This effect makes a meaningful fit of the ^{31}P MAS NMR lineshapes for the TiO_2-containing samples very difficult since significant overlap will occur between the various Q^n resonances. However, the TiO sample was fitted (Fig. 7(b) with 5% of the phosphorus sites existing as Q^1 species and the majority as Q^2, as would be expected from a metaphosphate stoichiometry.

The ^{23}Na MAS NMR spectra are shown overlaid in Fig. 7(c). The incorporation of the TiO_2 did not seem to have a significant effect on the sodium MAS NMR spectra of these samples. The lineshapes are broad and asymmetric with a tail on the low frequency side. This shape is characteristic of sodium observed in a glass where there is a spread of quadrupolar interactions [18,19]. Despite the lack of sharp features, a fit of these spectra is possible if multiple field data is considered, as in Fig. 7(d), with the disorder in the glass accounted for using a Gaussian distribution in C_Q (the quadrupolar coupling constant, a measure of the interaction between the nuclear spin magnetization and the electric field gradient), the width of which can be used as a semi-quantitative measure of disorder [20]. The multiple field data can be used to constrain things since under MAS there are effectively two residual interactions affecting the observed lineshape. There are residual second-order quadrupole effects and the spread of isotropic chemical shifts, often termed the chemical shift distribution. These interactions are, respectively, inversely and directly proportional (in Hz) to the applied magnetic field [21,22]. The parameters used for the simulations in Fig. 7(d) were a mean $C_Q = 2.0 \pm 0.1$ MHz, a FWHM Gaussian distribution in this parameter of $\Delta C_Q = (2.2 \pm 0.2)$ MHz and a mean isotropic chemical shift of $\delta_{iso} = -10 \pm 2$ ppm. This chemical shift value was kept constant and the asymmetry

parameter η_Q was kept at 0 for simplicity. In reality a distribution in C_Q would likely mean a distribution in these parameters also, but they usually have smaller effects.

3.3. Surface characterization

3.3.1. Surface roughness

The lowest roughness values obtained from both AFM and laser profilometry were observed for samples with the greatest content of TiO_2 (CNPT5), but still there were no significant difference between CNPT5 and CNP ($P = 0.1741$) or between CNPT5 and CNPT1 ($P = 0.0722$). However, the highest roughness was recorded for samples with 3 mol% TiO_2, which showed statistically significant differences from CNP ($P = 0.0345$) and CNPT5 ($P = 0.0077$). In addition, roughness measurements using Laser Profilometry revealed that there were no statistical differences between these latter two samples – Table 2, however this results could be affected by replication method, which does not reproduce features smaller than 0.1 μm, and at the same time it was the error of this method.

3.3.2. Wettability and surface free energy

There was no significant difference in the mean contact angle (°) between all tested compositions when using H_2O as a polar test liquid. However, using diiodomethane as a non-polar test liquid, the contact angles showed only significant differences with incorporation of the highest TiO_2 content in CNPT5 compared to TiO_2-free glasses. Moreover, this significant differences were also observed between CNPT1 and CNPT5 ($P = 0.0099$) and CNPT3 and CNPT5 ($P = 0.0121$) pairs. Generally, the observed contact angle values were significantly higher with diiodomethane compared to H_2O as given in Table 2.

Results of the total surface free energy for all tested samples were very similar and no statistical differences were observed between them. Moreover, in the analysis of the dispersive component, showed no significant differences observed between all these samples and CNP; for example, between CNP and CNPT1 ($P = 0.0509$), between CNP and CNPT3 ($P = 0.0818$), or between CNP and CNPT5 ($P = 0.4209$). Also, very close analysis showed that there were no significant differences between the polar part of surface free energy for all samples compared to the CNP; for example between CNP and CNPT1 ($P = 0.1624$), between CNP and CNPT3 ($P = 0.2979$), or between CNP and CNPT5 ($P = 0.3144$).

4. Discussion

This study aimed to produce glasses with controlled properties by adjusting the chemistry and to consider the change in physical and chemical properties known to play important roles in the success of biomaterials upon their placement in a physiological environment.

The observed increase in density due to replacement of Na_2O with TiO_2 is attributed to the replacement a light element (Na) with a heavier one (Ti). This increase in density was also associated with a significant increase in T_g that was used as a measure of the cross-link density of the glass network. The observed increase in the bulk density and T_g was believed to be due to the formation of TiO_5 or TiO_4 structural units and the formation of P–O–Ti bonds. This forms ionic cross-linking between the non-bridging oxygen of two different chains that strengthen the glass structure [27–29]. The density (ρ) and T_g for CNP glass with 40 mol% CaO is significantly higher than the comparable composition with 30 mol% CaO (2.58 ± 0.002 g cm^{-3}, 383 ± 1 °C). Furthermore, the addition of 5 mol% TiO_2 produced an even higher density and T_g compared to the system with 30 mol% CaO ($\rho = 2.63 \pm 0.001$ g cm^{-3}, $T_g = 451 \pm 3$ °C) [30]. Unlike all other studied compositions, 5 mol% TiO_2-containing glass showed two crystallization peaks. This finding suggested that TiO_2 could act as a nucleating agent and induce phase separation during cooling of the molten glass [13].

Incorporation of 5 mol% TiO_2 in the glass system $(CaO)_{40}(Na_2O)_5(P_2O_5)_{50}(TiO_2)_5$ reduced the degradation rate by two orders of magnitude in contrast to the one order of magnitude observed previously [30] for the same mol% of TiO_2 in a glass system with relatively lower CaO content $[(CaO)_{30}(Na_2O)_{15}(P_2O_5)_{50}(TiO_2)_5]$. Thus the findings in this study confirmed the hypothesis that incorporation of both TiO_2 with high CaO content will control the glass degradation properties. Moreover, the reduction in rate of degradation of the glasses used in this study with increasing TiO_2 content could be due to the formation of a highly cross-linked, dense structure that resists degradation as evidenced from the T_g and density data.

The reduction in degradation was associated with a concomitant reduction in the rate of release of all detected ions such as Ca^{2+}, Na^+, PO_4^{3-}, $P_3O_9^{3-}$, $P_2O_7^{4-}$, $P_3O_{10}^{5-}$, and Ti^{4+} Fig. (4). This indicates that the degradation and associated ion release can easily be tailored which in turn may improve cellular responses by controlling the rate of release of some beneficial ions such as Ca^{2+}, P^{5+}, and Ti^{4+}. The highest released anion species, $P_3O_9^{3-}$, suggested that a significant proportion of the $P_3O_9^{3-}$ was present in the original glass structure, a result were further demonstrated by the XRD analysis and reported previously [31]. The Ti^{4+} release was found to be inversely proportional to TiO_2 content and CNPT1 (the composition containing the lowest amount of TiO_2) released the highest amount of Ti^{4+},indicating that Ti^{4+} release is dependent on the glass degradation.

The significant rapid drop in pH associated with the CNP to acidic level could be due to the relatively higher degradation of this composition compared to the others. The higher degradation, in turn, was reflected with the higher level of release of different phosphate species into the degradation medium; the dissociation of these species resulted in the formation of phosphoric acid that produced an acidic environment [32]. However, in the remaining compositions, the pH remained relatively stable over the time scale of the experiment, although a decrease of approximately 1 pH unit was observed compared to the pH at $t = 0$ after a soaking period of 12–18 days. This was expected since the presence of Ti^{4+} in the glass resulted in increasing the cross-link density between the phosphate chains, which slowed down the hydration effects that was considered to be one of the processes responsible for the glass degradation [6]. When water gets into the glass, a gel layer usually formed on its surface, i.e., hydration. When this hydrated layer of phosphate chains leached into the surrounding medium, it undergoes hydrolysis and effectively releases PO_4^{3-} that eventually form H_3PO_4 acid and result in the drop in pH in the highly soluble Ti free glasses. For the remaining samples, CNPT1, CNPT3 and CNPT5, the change in pH was not drastic as marked as for CNP samples. These changes in pH will be expected to be smaller in a cell culture medium that is highly concentrated with ions and buffers [33] compared to H_2O used in this study for ease of detection of the released ions.

XPS analysis enabled evaluation of the chemical composition of the sample's top layer. This layer is in fact the first thin film which will be in contact with the media and cells when such a material is placed into the body. Reaction of the organic components from the body media and cell activity on the surface (attachment) start immediately and are connected with surface chemistry, topography and surface free energy [34,35]. For this reason it is important to know chemical composition of the top layer which could have an influence on further surface reactivity. The top thin film is composed of elements which were found in the bulk glass (Ca, Na, P, Ti and O), as well as carbon and nitrogen. Despite the samples being thoroughly cleaned before the test, the level of carbon contamina-

tion was rather high at 16–28%. This finding suggested that the surface reacted with the atmospheric carbon and nitrogen very quickly forming a thin contamination layer. It was observed that the sodium concentration was decreasing, which was in agreement with theoretical composition of the glasses. It was also found that with increasing titanium content, the amount of sodium decreased in the top layer. However, the total amount of titanium, which was recognized as titania, was lower than expected. This can be explained by the relatively large amount of contamination on the surface, which could affect the results. Nevertheless, no differences in chemical bonding were observed between the samples and all the elements were found mostly as oxides.

The FTIR spectra from the titanium-doped samples as a function of Ti^{4+} content showed to be different from that of titanium-free samples. This is because substituting Na_2O with TiO_2 increases the O/P ratio and introduces more Q^1 units into the structure at the expense of the Q^2 units associated with the metaphosphate composition. Also, as the Ti^{4+} content increases, the intensity of the bands associated with Q^2 groups decreases relative to those associated with Q^1 groups; however, a small shift of the ν_{as}(P–O–P) band to higher energy is observed as is a general broadening of the spectral features. The latter provides some evidence that the introduction of titanium ions increases the strength of the phosphate chains, whilst the former is related to both the extra structural disorder introduced by the inclusion of another cation and to the presence of Q^1 units necessary to charge balance the Ti^{4+} ions; a similar trend was observed in the infrared spectra from TiO_2–SnO_2–Li_2O–P_2O_5 glasses as a function of titanium content [36].

The ^{31}P NMR spectra show that the CNP samples consist mainly of Q^2 species, which is to be expected since the glasses contain 50 molar % P_2O_5 (i.e., it is a metaphosphate, and so should consist of infinite chains or loops of phosphate tetrahedra [37]. The presence of around 5% of the phosphorus sites in these samples exist as Q^1 species indicating some depolymerization, which has been previously observed in calcium metaphosphate glasses [38]. When TiO_2 is introduced to the system, the ^{31}P MAS NMR lineshape widens with increasing TiO_2 content. In light of the FTIR results, this is interpreted as an increasing amount of Q^1 species, their chemical shifts moved to a more negative value by the titanium cation. The ^{23}Na MAS NMR spectra of all three samples show identical lineshapes suggesting that the addition of titanium has very little effect on the sodium environment.

Not only the chemistry but also the topography of the surface of a biomaterial has a major influence on the interaction of biomaterials with cells starting initially with cell attachment which determines the subsequent processes like cell adhesion, spreading, morphology, migration, proliferation and differentiation [39]. Generally, the response of cells to surface topography differs according to cell type. Osteoblasts, for example, prefer rough surfaces, whereas fibroblasts favor smooth surfaces [34]. Hydrophilic rather than hydrophobic surfaces, on the other hand, supported adhesion of various cell types [35]. In this study, surface roughness, contact angles, and surface free energy were considered to give an indication about the surface topography and thermodynamic properties even though the initial surface is going to change throughout the degradation process, particularly for CNP glasses which are highly degradable.

Mean roughness R_a is an arithmetical mean deviation of the areas of all profile values of the roughness profile [40]. Depending on the expected roughness, the standards assume different cut-off and evaluation lengths. The expected R_a value for glass samples is in the range of 0.1–1 μm. For this reason, the minimum cut-off and evaluation length are 250 and 1250 μm, respectively; but preferably 800 and 4000 μm, respectively. Laser profilometry measurements satisfied the standard principles. However, due to the fact that the minimum cut-off length given by the standard is 80 μm (evaluation length 400 μm), AFM measurements conducted on the images of size 45 × 45 μm did not satisfy the standard principles. Nevertheless, measurements replicated the principles on a smaller scale giving results of roughness in the 'nanoscale' – R_a^{AFM}.

As seen from the results, the highest roughness was recorded for samples with 3 mol% TiO_2 as obtained from laser profilometry. On the nano-scale, however, there were no statistical differences between the roughness values recorded for all tested samples. This confirmed that the glass surface preparation provided comparable surface topography to avoid the influence of surface topography (roughness) on wetting ability measurement. Moreover, all the studied glass samples showed significantly higher roughness than the control Thermanox®.

In this study, static contact angles were measured where the measurement of the drop contact angle onto a flat surface for a certain time was considered. In this mode, the changes of the contact angle as a function of time are related only to evaporation and wetting ability of the surface. The contact angle measured using diiodomethane was the highest for these glasses. It is usually expected that a liquid with a lower surface tension will give rise to a smaller contact angle (diiodomethane in this study) on a given solid when compared to a liquid with a higher surface tension (water). This suggests that the chemical bonds between liquid and solid phases are stronger for this sample compared to the remaining samples, and this effect can be associated to the high reactivity of titanium. Moreover, this also indicated that the dominant effect was the polar characteristic of the phosphate glasses. This polarity can be attributed to the P–O–P bonds in the glass, and this was also supported in our previous studies [4,41].

Results of surface free energy determined for all tested samples were very similar and no statistical differences were observed between them which may suggest that the TiO_2 content had no effect on the wetting ability of the surface. All the glasses showed high wetting ability with relatively high SFE (~75 mN/m). However, the polar part of the energy is high which could suggest low bioactivity of the glasses [41].

5. Conclusion

The results showed that the small addition of TiO_2 to 40 mol% CaO contents sodium calcium phosphate glasses produced significantly higher density and glass transition temperature along with lower degradation compared to similar system with lower CaO content (30 mol%) and TiO_2-free glasses. These properties were also reflected in the released ions and the pH of the surrounding medium on soaking the glasses in water. TiP_2O_7, $NaCa(PO_3)_3$ and CaP_2O_6 phases were detected for the crystalline form of all TiO_2-containing glasses investigated throughout this study.

Chemistry of the surface assessed using XPS showed that the main surface elements were calcium, sodium, phosphorus, titanium and oxygen. With increasing titanium content an increase of titania in the top layer was observed. Nevertheless, the theoretical titanium content was higher than detected on the surface.

^{31}P MAS NMR results showed an increase in linewidth interpreted as an increase in Q^1 phosphorus species whose chemical shift occurs at a more negative position due to the effect of the titanium cation. ^{23}Na results suggest that the addition of TiO_2 to the system does not significantly affect the average sodium environment. Like NMR, FTIR also showed that substituting Na_2O with TiO_2 increases the strength of the phosphate chains, O/P ratio while it introduces more Q^1 units into the structure at the expense of the Q^2 units. On the other hand, TiO_2 content had no effect on the wetting ability of the surface as measured by surface free energy.

Acknowledgment

The authors would like to acknowledge the EPSRC for providing the funding to conduct this study (Grant Nos. EP/C004671/1, EP/C004698/1, and EP/C515560/1). MES thanks the EPSRC and University of Warwick for partially supporting the NMR equipment at Warwick.

References

[1] L.L. Hench, J.M. Polak, Science 295 (5557) (2002) 1014.
[2] I. Ahmed, C.A. Collins, M. Lewis, I. Olsen, J.C. Knowles, Biomaterials 25 (2004) 3223.
[3] E.A. Abou Neel, I. Ahmed, J.J. Blaker, A. Bismarck, A.R. Boccaccini, M.P. Lewis, S.N. Nazhat, J.C. Knowles, Acta Biomater. 1 (2005) 553.
[4] E.A. Abou Neel, I. Ahmed, J. Pratten, S.N. Nazhat, J.C. Knowles, Biomaterials 26 (2005) 2247.
[5] J.C. Knowles, J. Mater. Chem. 13 (2003) 2395.
[6] B.C. Bunker, G.W. Arnold, J.A. Wilder, J. Non-Cryst. Solids 64 (1984) 291.
[7] H. Gao, T. Tan, D. Wang, J. Control. Release 96 (2003) 21.
[8] B.C. Sales, R.S. Ramsey, J.B. Bates, L.A. Boatner, J. Non-Cryst. Solids 87 (1986) 137.
[9] V. Salih, K. Franks, M. James, G.W. Hastings, J.C. Knowles, J. Mater. Sci.: Mater. Med. 11 (2000) 615.
[10] M. Bitar, V. Salih, V. Mudera, J.C. Knowles, M. Lewis, Biomaterials 25 (2004) 2283.
[11] J.E. Gough, P. Christian, C.A. Scotchford, C.D. Rudd, I.A. Jones, J. Biomed. Mater. Res. 59 (2002) 481.
[12] J.E. Gough, P. Christian, C.A. Scotchford, I.A. Jones, J. Biomed. Mater. Res. 66A (2003) 233.
[13] A.S. Monem, H.E. ElBatal, E.M.A. Khalil, M.A. Azooz, Y.M. Hamdy, J. Mater. Sci.: Mater. Med., doi:10.1007/s10856-007-3044-3.
[14] E.A. Abou Neel, T. Mizoguchi, M. Ito, M. Bitar, V. Salih, J.C. Knowles, Biomaterials 28 (2007) 2967.
[15] D. Massiot, F. Fayon, M. Capron, I. King, S. Le Calvé, B. Alonso, J.-O. Durand, B. Bujoli, Z. Gan, G. Hoatson, Magn. Reson. Chem. 40 (2002) 70.
[16] T.F. Kemp, M.E. Smith, Solid State Nucl. Magn. Reson., doi:10.1016/j.ssnmr.2008.12.003.
[17] F. Fayon, D. Massiot, M.H. Levitt, J.J. Titman, D.H. Gregory, L. Duma, L. Emsley, S.P. Brown, J. Chem. Phys. 122 (2005) 194313-1.
[18] S.C. Kohn, R. Dupree, M.E. Smith, Geochim. Cosmochim. Acta 53 (1989) 2925.
[19] S.C. Kohn, M.E. Smith, P.J. Dirken, E.R.H. Van Eck, A.P.M. Kentgens, R. Dupree, Geochim. Cosmoschim. Acta 62 (1998) 79.
[20] L.A. O'Dell, S.L.P. Savin, A.V. Chadwick, M.E. Smith, Appl. Magn. Reson. 32 (2007) 527.
[21] M.E. Smith, E.R.H. Van Eck, Prog. NMR Spectrosc. 34 (1999) 159.
[22] K.J.D. MacKenzie, M.E. Smith, Multinuclear Solid State NMR of Inorganic Materials, Pergamon, 2002.
[23] D. Ilieva, B. Jivov, G. Bogachev, C. Petkov, C. Penkov, Y. Dimitriev, J. Non-Cryst. Solids 283 (2001) 195.
[24] Y.M. Moustafa, K. El-Egili, J. Non-Cryst. Solids 240 (1998) 144.
[25] J.O. Byun, B.H. Kim, K.S. Hong, H.J. Jung, S.W. Lee, A. Izyneev, J. Non-Cryst. Solids 190 (1995) 288.
[26] P.-Y. Shih, H.-M. Shiu, Mater. Chem. Phys. 106 (2007) 222.
[27] P.K. Brow, D.R. Tallant, W.L. Warren, A. McIntyre, D.E. Day, Phys. Chem. Glasses 38 (1997) 300.
[28] V. Rajendran, A.V. Gayathri Devi, M. Azooz, F.H. El-Batal, J. Non-Cryst. Solids 353 (2006) 77.
[29] T. Kasuga, Y. Abe, J. Non-Cryst. Solids 243 (1999) 70.
[30] E.A. Abou Neel, J.C. Knowles, J. Mater. Sci.: Mater. Med., doi:10.1007/s10856-007-3079-5.
[31] I. Ahmed, M.P. Lewis, S.N. Nazhat, J.C. Knowles, J. Biomater. Appl. 20 (2005) 65.
[32] J.R.V. Wazer, K.A. Holst, J. Am. Ceram. Soc. 72 (1950) 639.
[33] W. Chrzanowski, E.A. Abou Neel, D.A. Armitage, J.C. Knowles, Acta Biomater. 4 (2008) 1969.
[34] L. Ponsonnet, K. Reybier, N. Jaffrezic, V. Comte, C. Lagneau, M. Lissac, et al., Mater. Sci. Eng. C 23 (2003) 551.
[35] C. Wirth, B. Grosgogeat, C. Lagneau, N. Jaffrezic-Renault, L. Ponsonnet, Mater. Sci. Eng. C 28 (6) (2008) 990.
[36] H. Schweikl, R. Müller, C. Englert, K.-A. Hiller, R. Kujat, M. Nerlich, G. Schmalz, J. Mater. Sci.: Mater. Med. 18 (2007) 1895.
[37] R.K. Brow, R.J. Kirkpatrick, G.L. Turner, J. Non-Cryst. Solids 16 (1990) 39.
[38] J.P. Fletcher, R.J. Kirkpatrick, D. Howell, S.H. Risbud, J. Chem. Soc. Faraday Trans. 89 (1993) 3297.
[39] T.P. Kunzler, T. Drobek, M. Schuler, N.D. Spencer, Biomaterials 28 (2007) 2175.
[40] ISO 4288, Geometrical Product Specifications (GPS) – Surface texture: Profile method – Rules and procedures for the assessment of surface texture, 1996.
[41] E.A. Abou Neel, L.A. O'Dell, M.E. Smith, J.C. Knowles, J. Mater. Sci.: Mater. Med., doi:10.1007/s10856-007-3313-1.